CPP

Contributions to Plasma Physics

www.cpp-journal.org

WILEY-VCH

REPRINT

Contrib. Plasma Phys. **56**, No. 6-8, 495 – 503 (2016) / **DOI** 10.1002/ctpp.201610060

Recent Developments in Plasma Edge Theory

W. M. Stacey*

Georgia Institute of Technology, Atlanta, GA 30332 USA

Received 01 September 2015, revised 08 October 2015, accepted 23 October 2015
Published online 08 July 2016

Key words Pinch, intrinsic rotation, plasma edge, radial electric field, ion orbit loss.

Recent developments in electromagnetic particle pinch, ion orbit loss, intrinsic rotation, rotation theory and radial electric field theory in the tokamak plasma edge are described.

1 Introduction

This paper reviews a concerted effort over several years by the Georgia Tech plasma group, in collaboration with colleagues at DIII-D and elsewhere, to develop a more complete physics model for the plasma edge. Recent work on i) the non-diffusive transport effects arising from electromagnetic particle pinches, ii) momentum-conserving pinch-diffusion theory, iii) the determination of the radial electric field, iv) the effects of 3D magnetic fields on edge rotation theory, v) determination of experimental deuterium rotation velocities and vi) ion-orbit-loss and X-loss/transport effects and intrinsic rotation are summarized.

2 Fluid moment equations

The first three velocity moments of the steady-state Boltzmann transport equation describing the distribution function for species j are the continuity equation

$$\nabla \cdot n_j V_j \equiv \nabla \cdot \Gamma_j = S^0_{nbj} + n_{oj} n_e \langle \sigma_{ion} \upsilon \rangle_j = S^0_{nbj} + n_e \nu_{ionj} = S^0_j \tag{1}$$

the momentum balance equation (with $n_j m_j V_j \times$ Eq. (1) subtracted to simplify the first term)

$$n_j m_j (V_j \cdot \nabla) V_j + \nabla p_j + \nabla \cdot \Pi_j = n_j e_j (E + V_j \times B) + F^1_j + (S^1_j - m_j V_j S^0_j) \tag{2}$$

the energy balance equation

$$\nabla \cdot Q_j \equiv \nabla \cdot (q_j + 1.5 \Gamma_j T_j) = S^2_{nbij} - \sum_{k \neq j} F^2_{jk} - 1.5 n_j n_e \langle \sigma_{cx} \upsilon \rangle (T_j - T_{oj}) \tag{3}$$

and, as a surrogate for the very complex fourth moment equation, the closure relation

$$q_j = -n_j \chi_j \nabla T_j. \tag{4}$$

Here n, m, e, T, V refer to density, mass, charge, temperature and fluid velocity, q is conductive heat flux, p is the pressure, Π is the viscous stress tensor, S indicates a source and F indicates a velocity moment of the collision operator summed over other species present. Ionization and charge-exchange are represented by the ion and cx subscripts, and the oj subscript indicate a neutral atom of species j. E and B are the electric and magnetic fields. When $j = e$ the last term in Eq. (3) is replaced by the radiation power loss term $-n_e \sum_k n_k L_k(T_e)$, where L_k is the radiative emissivity for species "k". The numerical superscript indicates the velocity moment. For example S^0_{nbj} indicates the zeroth velocity moment of the neutral beam (or other external particle source) deposition into the plasma—the neutral beam particle source, S^1_{nbj} represents the neutral beam or other external momentum source, and S^2_{nbj} represents the second velocity moment of the neutral beam (or other external energy source) deposition (i.e. the neutral beam heating of species j).

* Corresponding author. E-mail: weston.stacey@nre.gatech.edu, Phone: +01 404 894 3714, Fax: +01 404 894 3733

3 Electromagnetic particle pinch [1]

The radial ion particle flux transported through the edge plasma is the resultant of two large components, an outward diffusion flux driven by the pressure gradient and a usually inward pinch flux driven mainly by electromagnetic E and $V \times B$ forces. When the Lorentz approximation for the collisional momentum exchange between species j and all other species k, $F_j^1 = -n_j m_j \sum_k \nu_{jk}(V_j - V_k)$ is used, the flux surface average (FSA) viscosity term is written [1] as $\langle R^2 \nabla\varphi \cdot \nabla \cdot \Pi \rangle = R_0 n_j m_j \nu_{visj} V_{\varphi j}$ and the FSA of the inertial term as $\langle R^2 \nabla\varphi \cdot n_j m_j (V_j \cdot \nabla) V_j \rangle = R_0 n_j m_j \nu_{inj} V_{\varphi j}$, the toroidal momentum balance equations for a two-ion-species plasma may be written [1]

$$B_\theta e_j \Gamma_{rj} = n_j m_j (\nu_{dj} + \nu_{jk}) V_{\varphi j} - n_j m_j \nu_{jk} V_{\varphi k} - (S_{\varphi j}^1 + n_j e_j E_\varphi^A) \tag{5}$$

(where $S_{\varphi j}^1$ is toroidal momentum input and $\nu_{dj} \equiv \nu_{visj} + \nu_{inj} + \nu_{cxj}$), which can be combined with the radial momentum balance equations

$$E_r = B_\theta V_{\varphi j} - B_\varphi V_{\theta j} - \frac{1}{n_j e_j} \frac{\partial p_j}{\partial r} \tag{6}$$

to obtain the pinch-diffusion expression for the radial ion particle flux that is required by momentum balance

$$\Gamma_{rj} = n_j D_{jj} L_{pj}^{-1} - n_j D_{jk} L_{pk}^{-1} + n_j V_{rj}^{pinch} \tag{7}$$

where $D_{jj} \equiv m_j T_j (\nu_{dj} + \nu_{jk})/(e_j B_\theta)^2$, $D_{jk} \equiv (m_j T_k \nu_{jk})/(e_j e_k B_\theta^2)$, $L_X^{-1} \equiv -(\partial X/\partial r)/X$ and

$$n_j V_{rj}^{pinch} \equiv -\frac{S_{\varphi j}^1}{e_j B_\theta} - \frac{n_j E_\varphi^A}{B_\theta} - \frac{n_j m_j}{e_j B_\theta} \left[(\nu_{dj} + \nu_{jk}) \left(\frac{E_r}{B_\theta} + \frac{B_\varphi}{B_\theta} V_{\theta j} \right) - \nu_{jk} V_{\varphi k} \right] \tag{8}$$

is the (mostly) electromagnetic pinch flux. If we assume $L_{Tk}^{-1} \simeq L_{Tj}^{-1}$ and $L_{nk}^{-1} \simeq L_{nj}^{-1}$, Eq. (7) can be simplified [1] to

$$\Gamma_{rj} \simeq n_j D_j L_{pj}^{-1} + n_j V_{rj}^{pinch}, D_j \equiv (m_j T_j \nu_{jk}/(e_j B_\theta)^2)(1 + \nu_{dj}/\nu_{jk} - e_j/e_k). \tag{9}$$

Differences in the pinch velocity were found to be associated with dramatic differences in performance in several otherwise similar discharge conditions in DIII-D. The change in the pinch velocity was evaluated from experimental data across the L-H transition [2]. In L-mode, just prior to the transition, the pinch velocity was weakly inward, with large outward E_r and inward V_θ contributions that almost canceled. However, after the transition E_r switched to negative and the E_r contribution changed to inward, adding to the V_θ contribution to produce a large inward pinch velocity which was maintained throughout the H-mode phase. The pinch velocities in the L- and H-mode are shown in Fig. 1.

In two otherwise matching DIII-D shots in one of which RMP coils were on, the negative E_r was somewhat reduced by the RMP coils, which in turn reduced the inward particle pinch as shown in Fig. 2, resulting in a lower edge density below the ELM threshold and consequently in ELM suppression [3]. Comparing Fig. 1 and Fig. 2 suggests that dropping temporarily into L-mode might also suppress ELMs.

Evaluation of the separate diffusive and non-diffusive (pinch) radial particle flux components for two different RMP shots [4] and for several times in the interval between ELMs in an H-mode discharge [5] revealed that the net outward radial particle flux resulted from the near cancellation of much larger outward diffusive fluxes and inward pinch fluxes, as shown in Fig. 3 for two different RMP shots.

Many analyses of the radial ion flux in the plasma edge are made (incorrectly) with pure diffusion theory, which is the total flux shown by the upper curves in Fig. 3, by adjusting the diffusion coefficient to match the measured density or particle flux determined from the continuity equation (the middle curves). It is clear from comparing the upper and middle curves that a very small adjusted diffusion coefficient that varied with radius inversely as the upper curves would be necessary, which result has been (questionably) interpreted as a particle "transport barrier". The inappropriateness of a purely diffusive radial particle flux model is further attested by the inward radial ion flux observed experimentally as the edge pedestal rebuilds just after an ELM crash [5], which would require a negative diffusion coefficient.

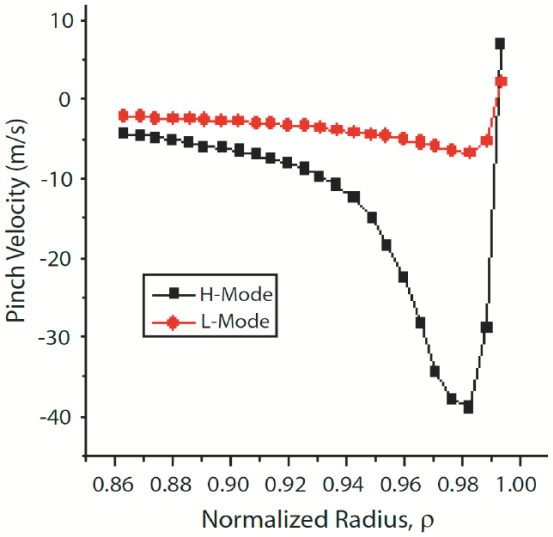

Fig. 1 Experimental particle pinch velocity for L-mode and ELM-free H-mode phases [2].

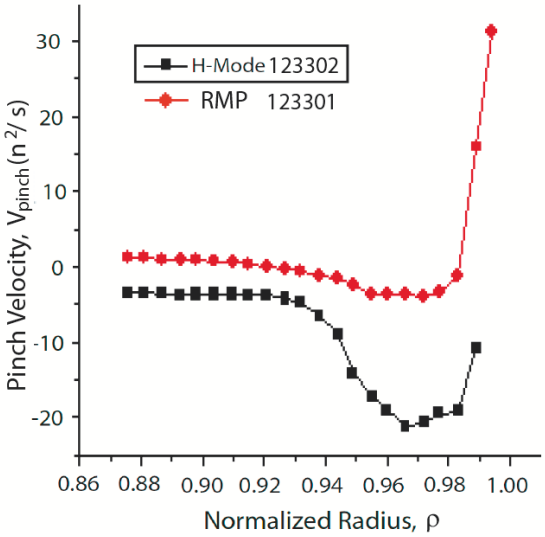

Fig. 2 Experimental particle pinch velocity for DIII-D H-mode and RMP discharges [3].

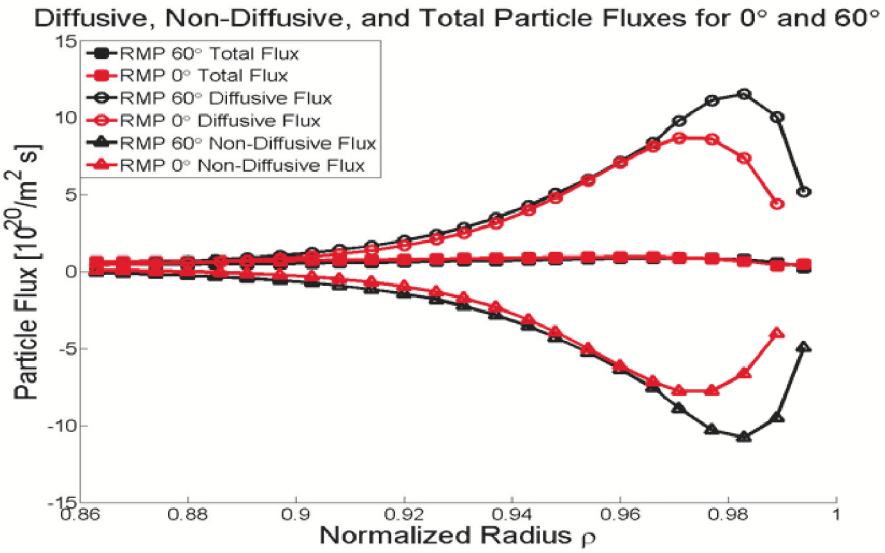

Fig. 3 Diffusive and pinch radial particle fluxes for two DIII-D RMP discharges [4].

4 A particle pinch-diffusion theory that conserves momentum

A systematic procedure for deriving a new particle diffusion theory which is consistent with momentum conservation is to solve the momentum balance equation for the particle flux and then substitute this form for the particle flux into the continuity equation [1, 6]. While this can be done with the particle flux of Eq. (7), the result is a coupled set of diffusion equations for the densities of all ion species in the plasma [1], and this is too complicated for a first step. Instead, we have focused on the approximate form of Eq. (9), which when substituted into the radial component of Eq. (1) yields for a 1D radial diffusion equation in cylindrical geometry

$$(\nabla \cdot \Gamma)_r = \frac{1}{r}\frac{\partial\left(r\left\{\frac{D_j}{T_j}\frac{\partial(n_j T_j)}{\partial r} + n_j V_{rj}^{pinch}\right\}\right)}{\partial r} = S_j^0 \tag{10}$$

Using a procedure similar to that used above to derive V_{rj}^{pinch}, a $V_{\theta j}^{pinch}$ can be derived from the poloidal momentum balance and a 2D $(r-\theta)$ diffusion equation in toroidal geometry can be obtained [where $h = (1+(r/R)cos(\theta))$]

$$(\nabla\cdot\Gamma)_\theta = \frac{1}{rRh}\frac{\partial\left(rRh\left\{\frac{D_j}{T_j}\frac{\partial(n_jT_j)}{\partial r}+n_jV_{rj}^{pinch}\right\}\right)}{\partial r}+\frac{1}{r}\frac{\partial\left(Rh\left\{\frac{D_j}{T_j}\frac{1}{r}\right\}\frac{\partial(n_jT_j)}{\partial\theta}+n_jV_{\theta j}^{pinch}\right)}{\partial\theta} = S_j^0 \tag{11}$$

5 Radial electric field [7]

Combining the summed multiple ion and electron momentum balance equations using an interspecies friction term of the form $F_{ei} = -nm\nu_{ei}(V_e-V_i) = -\eta n^2e^2(V_e-V_i) = ne\eta j$ leads to [7]

$$E = \eta j - u\times B - \frac{\nabla p_e}{ne}+\frac{j\times B}{ne} = \eta j - u\times B+\frac{\nabla p_i}{ne} \tag{12}$$

where $u = (n_im_iV_i+n_em_eV_e)/(n_im_i+n_em_e)$, with a sum over ion species "i" being understood. Making use of the leading order plasma force balance $j\times B = \nabla p = \nabla p_i+\nabla p_e$ yields another form of Ohms Law for the determination of the electric field in a rotating plasma shown in the second of Eqs. (12). The first form of Eq. (12) provides an insight into how the radial electric field (and hence the quantities such as ion orbit loss, radial ion flux and rotation that depend upon it) might be controlled by creating a poloidal or toroidal current in the plasma, most likely in the edge plasma.

It should be possible to pull all of the foregoing together into self-consistent "first-principles" calculations for the radial particle flux, rotation velocities and radial electric field [7]. The particle sources, ion-orbit- and X-loss, and radial diffusive and non-diffusive (electromagnetic pinch, X-transport) transport processes and the return currents necessary to maintain charge neutrality should determine the radial particle flux. The radial particle flux, in turn, provides a torque which, together with any external torque, determines the rotation velocities, which must then be corrected by intrinsic rotation due to ion orbit loss. The rotation velocities determine the motional electric field, which in turn affects the ion-orbit-loss and X-loss, which affect the rotation velocities, etc. The practical aspects of making such self-consistent sets of calculations and comparing them with experiment are being examined in an ongoing PhD thesis [8].

6 Viscous damping of toroidal rotation and poloidal asymmetries in the edge plasma [9,10]

The viscous damping of toroidal angular momentum is represented by the flux surface average (FSA) of the toroidal component of the viscous torque [9]

$$\langle R^2\nabla\phi\cdot\nabla\cdot\Pi\rangle = \frac{1}{V'}\frac{\partial}{\partial\psi}(V'\langle R^2\nabla\phi\cdot\Pi\cdot\nabla\psi\rangle) = \langle\frac{1}{Rh_p}\frac{\partial}{\partial l_\psi}(R^2h_p\pi_{\psi\phi})\rangle \tag{13}$$

where V' is the differential volume between flux surfaces and h_p is the poloidal metric element.

The Braginskii decomposition of the viscous rate of strain tensor [11] has been generalized [12,13] to toroidal flux surface geometry and arbitrary collisionality with 3D toroidally non-symmetric magnetic fields by writing the elements of the general rate of strain tensor of fluid theory

$$W_{\alpha\beta}\equiv\hat n_\alpha\cdot\nabla V\cdot\hat n_\beta+\hat n_\beta\cdot\nabla V\cdot\hat n_\alpha-\frac{2}{3}\delta_{\alpha\beta}\nabla\cdot V = \left(\frac{\partial V_\beta}{\partial l_\alpha}+\sum_k\Gamma_{\beta k}^\alpha V_k\right)+\left(\frac{\partial V_\alpha}{\partial l_\beta}+\sum_k\Gamma_{\alpha k}^\beta V_k\right)-\frac{2}{3}\delta_{\alpha\beta}\nabla\cdot V \tag{14}$$

where $\Gamma_{\beta k}^\alpha$ are the Christoffel symbols. The viscous stress tensor elements can be decomposed into "parallel", "gyroviscous" and "perpendicular" components with viscosity coefficients which differ by several orders of magnitude $(\eta_0\gg\eta_{3,4}\simeq\eta_0/\Omega\tau\gg\eta_{1,2}\simeq\eta_0/(\Omega\tau)^2)$

$$\pi_{\alpha\beta} = -\eta_0W_{\alpha\beta}^0+[\eta_3W_{\alpha\beta}^3+\eta_4W_{\alpha\beta}^4]-[\eta_1W_{\alpha\beta}^1+\eta_2W_{\alpha\beta}^2]\equiv\pi_{\alpha\beta}^0+\pi_{\alpha\beta}^{34}+\pi_{\alpha\beta}^{12} \tag{15}$$

where, denoting $f_\alpha \equiv B_\alpha/|B|$, the leading order parallel viscosity contribution $\pi^0_{\psi\phi} = -\eta_0 W^0_{\psi\phi} = -3/2\eta_0 f_\psi f_\varphi H^0(V_\varphi, V_\theta)$ vanishes in the absence of radial magnetic fields ($f_{\psi=r} \equiv B_{\psi=r}/|B| = 0$), where $H^0(V_\varphi, V_\theta)$ depends upon the flows and their gradients [9, 10] , leaving the gyroviscous $[\eta_3 W^3_{\alpha\beta} + \eta_4 W^4_{\alpha\beta}]$ contribution [12]

$$\langle R^2 \nabla\phi \cdot \nabla \cdot \Pi \rangle = -\left\langle \frac{1}{R h_p} \frac{\partial}{\partial l_\psi} \left(R^3 h_p \eta_4 \frac{\partial (V_{\varphi/R})}{\partial \ell_p} \right) \right\rangle_{g\nu} \tag{16}$$

as the largest surviving term in the viscous torque of Eq. (9) for axisymmetric tokamaks with $f_{\psi=r} \equiv B_{\psi=r}/|B| = 0$. This formalism predicts toroidal rotation velocities in reasonable agreement with experiment [12, 13] in the central plasma, but seems to break down in the plasma edge.

However, when $f_\psi \neq 0$, leading order (η_0) terms survive in Eq. (13), yielding a general form for the leading order parallel contribution to the toroidal angular momentum viscous damping term [10]

$$\left\langle R^2 \nabla\varphi \cdot \nabla \cdot \Pi_0 \right\rangle = -\frac{3}{2} \left\langle \frac{1}{R h_p} \frac{\partial (R^2 h_p \eta_0 f_\psi f_\varphi H^0)}{\partial \ell_\psi} \right\rangle = \frac{3}{2} \left\langle R \eta_0 f_\psi f_\varphi H^0 L^{-1}_\psi \right\rangle \tag{17}$$

$$L^{-1}_\psi \equiv -\left\{ \frac{1}{H_0} \frac{\partial H^0}{\partial \ell_\psi} + \frac{1}{f_\psi} \frac{\partial f_\psi}{\partial \ell_\psi} + \frac{1}{f_\varphi} \frac{\partial f_\varphi}{\partial \ell_\psi} + \frac{1}{\eta_0} \frac{\partial \eta_0}{\partial \ell_\psi} + \frac{1}{h_p} \frac{\partial h_p}{\partial \ell_\psi} + \frac{2}{R} \frac{\partial R}{\partial \ell_\psi} \right\} \tag{18}$$

is a composite of inverse radial gradient scale-lengths of flow velocities, densities, temperature, magnetic fields and the flux surface geometry. Note that the sign of $f_\varphi \equiv B_\varphi/|B|$ is >0 when the toroidal field is parallel to the plasma current and <0 when it is anti-parallel, as in the representation of this paper.

A rotation theory [12–14] has been developed based on Eq. (16), evaluation of which requires the calculation of poloidal flow and density asymmetries using a lowest order Fourier series expansion of the continuity and poloidal momentum balance equations. This theory has been developed for circular [12] and elongated [13, 14] plasma models and applied to calculate poloidal asymmetries and rotation velocities in DIII-D [12, 13] and K-STAR [15]. While the calculated poloidal asymmetries are small and the rotation velocities are in reasonable agreement with measured values in the core plasma, the calculated asymmetries become questionable in the edge plasma. Radial magnetic field components would be expected to be strongest in the plasma edge and are at least in part responsible for the rotation velocities in the edge plasma, and we have recently initiated an extension of the theory in this area [9, 10]. Various representations of $f_\psi \equiv B_\psi/|B|$ have been discussed in the literature (e.g. [16]).

7 "Experimental" deuterium rotation velocities

Directly measured deuterium rotation velocities are not routinely available, so for interpretive analysis it is frequently necessary to construct these quantities using the data that are measured and auxiliary calculations. It is frequently, but not always, observed that when the carbon (k) and deuterium (j) toroidal velocities are measured [17] they are similar, which supports a perturbation calculation with the difference $\Delta V_\varphi \equiv (V_{\varphi j} - V_{\varphi k})$ as the small parameter [18]. If $|\Delta V^1_\varphi| \ll |V^{meas}_{\varphi k}|$, the perturbation approach should be valid.

In leading (zero) order $\Delta V^0_\varphi = 0$ and Eqs. (1) may be solved for $\nu^0_{dj} = \nu^0_{dk} \equiv \nu^0_d$

$$\nu^0_d = [(n_j e_j (E^4_\varphi + B_\theta V_{rj}) + S^1_{\varphi j}) + (n_k e_k (E^A_\varphi + B_\theta V_{rk}) + S^1_{\varphi k})]/[(n_j m_j + n_k m_k) V^{meas}_{\varphi k}] \tag{19}$$

and then to first order

$$\Delta V^1_\varphi = \frac{(n_j e_j (E^A_\varphi + B_\theta V_{rj}) + S^1_{\varphi j}) - n_j m_j \nu^0_{dj} V^{meas}_{\varphi k}}{n_j m_j (\nu^0_{dj} + \nu_{jk})} \tag{20}$$

$$\nu^1_{dj} = \nu^0_d, \qquad \nu^1_{dk} = \frac{(n_k e_k (E^A_\varphi + B_\theta V_{rk}) + S^1_{\varphi k}) + n_k m_k \nu_{kj} \Delta V^0_\varphi}{n_k m_k V^{meas}_{\varphi k}} \tag{21}$$

Using the radial electric field calculated from the carbon radial momentum balance of Eq. (6) with $j = k$ in which all the quantities on the right side are measured, and the "experimental" deuterium toroidal velocity from

$V_{\phi j}^{exp} = V_{\varphi k}^{meas} + \Delta V_{\varphi}^{1}$ in the radial momentum balance for deuterium yields an "experimental" value for the deuterium poloidal rotation velocity [17]

$$V_{\theta j}^{exp} = \frac{[B_\theta V_{\varphi j}^{exp} - E_r - \frac{1}{n_j e_j}\frac{\partial p_j}{\partial r}]}{B_\varphi} \tag{22}$$

8 Ion orbit loss, intrinsic rotation and X-transport

8.1 Basic ion orbit loss calculation [19, 20]

The basic ion orbit loss calculation is of the minimum energy an ion located at a particular poloidal position (ψ_0, θ_0) on an internal flux surface ψ_0 with a direction cosine ζ_0 relative to the toroidal magnetic field direction must have in order to be able to execute an orbit that will cross the separatrix at location (ψ_{sep}, θ_{sep}). We use the conservation of canonical toroidal angular momentum

$$RmV_\parallel f_\varphi + e\psi = const = R_0 m V_{\parallel 0} f_{\varphi 0} + e\psi_0 \tag{23}$$

as the orbit constraint for an ion at a location (ψ_0, θ_0) with parallel velocity $V_{\parallel 0} \equiv \zeta_0 V_0$,where $f_\varphi = |B_\varphi / B|$, R is the major radius and ψ is the flux surface value. Requiring also the conservation of energy and of magnetic moment

$$\frac{1}{2}m(V_\parallel^2 + V_\perp^2) + e\phi = const = \frac{1}{2}m(V_{\parallel 0}^2 + V_{\perp 0}^2) + e\phi_0 \equiv \frac{1}{2}mV_0^2 + e\phi_0 \,,\ \frac{mV_\perp^2}{2B} = const = \frac{mV_{\perp 0}^2}{2B_0} \tag{24}$$

leads to an equation for the minimum speed $V_0 \equiv \sqrt{V_{0\perp}^2 + V_{0\parallel}^2}$ for which an ion at (ψ_0, θ_0) with direction cosine ζ_0 relative to the magnetic field can access an orbit that can reach the point (ψ_s, θ_s) on the separatrix (or other loss surface)

$$V_0^2\left[\left(\left|\frac{B_s}{B_0}\right|\frac{f_{\varphi 0}}{f_{\varphi s}}\zeta_0\right)^2 - 1 + \left(1-\zeta_0^2\right)\left|\frac{B_s}{B_0}\right|\right] + V_0\left[\frac{2e(\psi_0-\psi_s)}{Rmf_{\varphi s}}\left(\left|\frac{B_s}{B_0}\right|\frac{f_{\varphi 0}}{f_{\varphi s}}\zeta_0\right)\right] \quad + \\ \left[\left(\frac{e(\psi_0-\psi_s)}{Rmf_{\varphi s}}\right)^2 - \frac{2e(\phi_0-\phi_s)}{m}\right] \quad = \quad 0 \tag{25}$$

In the GTEDGE code (a background modeling and experimental data interpretation code), this equation is solved many times for each of 8 values of θ_s , 8 values of θ_0, 22 values of ζ_0 over -1< ζ_0 <1 and 24 values of ρ_0 , using experimental radial electric field and ion temperature gradients in order to generate the minimum physically realistic value of $E_{min}(\zeta_0, \rho_0, \theta_0, \theta_s) = 1/2 m V_{0min}^2(\zeta_0, \rho_0, \theta_0, \theta_s)$ as input for the IOL numerical computational strategy [20], which takes into account that ions could spiral about the flux surface many times in the time required to be transported radially to the next flux surface in determining the ion orbit loss. Once the minimum loss energy $E_{min}(\rho_0, \zeta_0)$ for ions on internal surface ρ_0 with direction cosine ζ_0 is determined by one of the computational strategies [19, 20], the cumulative loss fraction that has taken place over $0 < \rho < \rho_0$ of the total ion population with directions cosine ζ_0 that would have been present in the absence of IOL can be calculated from

$$F_{loss}(\rho_0) = \frac{\int_{-1}^{1} d\zeta_0 \int_{V_0^{\min}(\rho_0,\zeta_0)}^{\infty} f(V_0) V_0^2 dV_0}{\int_{-1}^{1} d\zeta_0 \int_0^{\infty} f(V_0) V_0^2 dV_0} = \frac{\int_{-1}^{1} d\zeta_0 \int_{\varepsilon_{\min}(\rho_0,\zeta_0)}^{\infty} \varepsilon^{1/2} e^{-\varepsilon} d\varepsilon}{\int_{-1}^{1} d\zeta_0 \int_0^{\infty} \varepsilon^{1/2} e^{-\varepsilon} d\varepsilon} = \frac{\int_{-1}^{1} d\zeta_0 \Gamma(\frac{3}{2}, \varepsilon_{\min}(\rho_0, \zeta_0))}{2\Gamma(\frac{2}{3})} \tag{26}$$

where $\varepsilon_{\min}(\rho_0, \zeta_0) \equiv E_{\min}(\rho_0, \zeta_0)/kT_{ion}(\rho_0)$, $\Gamma(3/2)$ is the complete gamma function of order 3/2, $\Gamma(n, a) = \Gamma(n) - \gamma(n, a)$ and $\gamma(n, a)$ and is the incomplete gamma function of order n and argument a. These forms result

from the use of a Maxwellian distribution to evaluate the integrals. Similar derivations lead to the cumulative fractions of ion energy and momentum that are IOL lost from within flux surface ρ_0 (i.e. for $0 < \rho \leq \rho_0$)

$$E_{loss}(\rho_0) = \frac{\int_{-1}^{1} d\zeta_0 \Gamma(\frac{5}{2}, \varepsilon_{\min}(\rho_0, \zeta_0))}{2\Gamma(\frac{5}{2})} \ , \ M_{loss}(\rho_0) = \frac{\int_{-1}^{1} d\zeta_0 \Gamma(2, \varepsilon_{\min}(\rho_0, \zeta_0))\zeta_0}{2\Gamma(2)} \tag{27}$$

As shown in Fig. 4, the fraction of ions and ion energy leaving the plasma on loss orbits is large in the edge. These lost ions and ion energy are deposited primarily in the SOL near the outboard midplane [20].

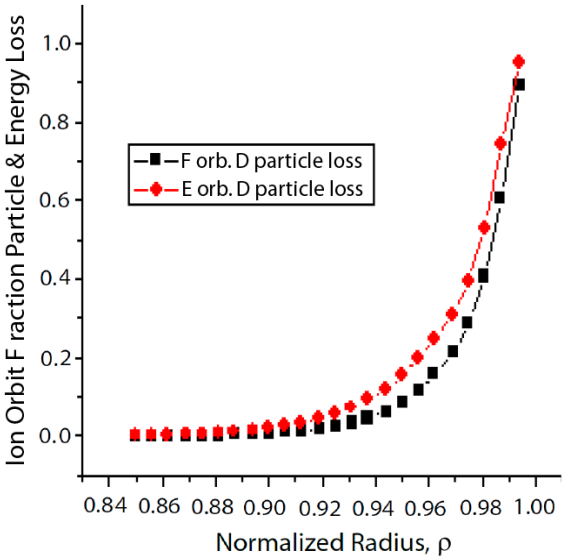

Fig. 4 Ion orbit loss fractions for particles and energy for DIII-D discharge 149468 [17].

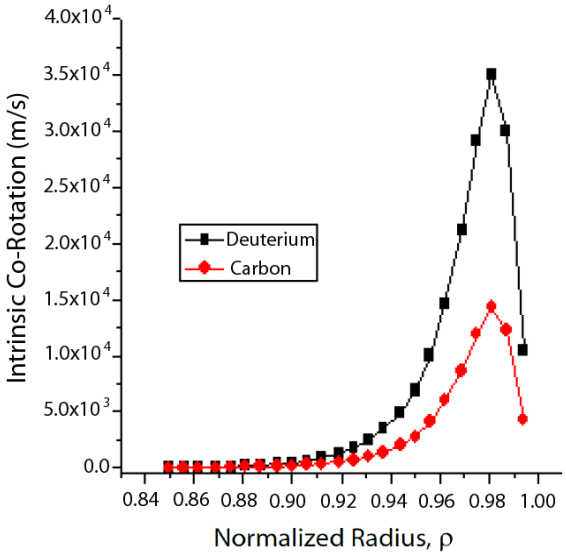

Fig. 5 Calculated intrinsic co-rotation of deuterium ions produced by ion orbit loss [17].

The fraction of outflowing thermalized ions lost by ion orbit loss within the differential volume between the flux surfaces at ρ_k and ρ_{k-1} may be determined by subtraction $dF_{loss}(\rho_k) = F_{loss}(\rho_k) - F_{loss}(\rho_{k-1})$ (similarly for dE_{loss} and dM_{loss}). In the slab approximation the IOL thermal ion loss constitutes a loss rate $-\Gamma(\rho)(\partial F_{loss}/\partial\rho)$ in the continuity equation for the outward thermal ion flux, which must be balanced by an inward current of ions from the SOL $\partial\Gamma_{comp}(\rho)/\partial\rho = -\Gamma(\rho)(\partial F_{loss}/\partial\rho)$. If thermal ions are being deposited by NBI at a rate $S_{nbi}(1 - f^{nb}_{loss})$, where f^{nb}_{loss} is the IOL loss rate of the fast NBI ions, there must be an inward current of thermal ions from the SOL to compensate the loss current of fast NBI ions $(\partial\Gamma_{comp}/\partial\rho)_{nb} = -(\partial\Gamma^{f}_{nb}/\partial\rho) = -S_{nb}f^{nb}_{loss}$. Thus, including the ionization of neutrals S_{ion} , the (slab) continuity equation including IOL is

$$\partial\Gamma(\rho)/\partial\rho = (S_{ion}(\rho)) + S_{nb}(\rho)(1 - 2f^{nb}_{loss}(\rho)) - 2(\partial F_{loss}(\rho)/\partial\rho)\Gamma(\rho) \tag{28}$$

8.2 Intrinsic rotation [17, 19, 20, 20, 21]

The preferential loss of counter-current ions leaves the edge plasma with a predominant co-current ion population, the net current resulting from which can be calculated from

$$\Delta V_{\|}(\rho, \zeta_0) = 2\pi^{-1/2} M_{loss}(\rho, \zeta_0)\sqrt{2kT_{ion}(\rho)/m} \tag{29}$$

This phenomenon causes an increasing with radius co-current toroidal rotation out to the radius slightly inside the LCFS at which the ctr-current ions have almost all been lost. Beyond this radius the small loss of co-current ions begins to increase, reducing the predominance of co-current ions remaining in the plasma and thus producing the peaking in intrinsic rotation shown in Fig. 5 and measured in this [17] and other discharges.

8.3 X-loss and X-transport [22]

In a region inside the separatrix about the X-point the poloidal field is very small, $B_\theta \ll \varepsilon B_\phi$ (Fig. 6), and the field lines are almost purely toroidal and do not spiral poloidally about the tokamak to provide the usual neoclassical cancellation of drift effects. Ions spiral poloidally over the remainder of the flux surface outside of this "X-region" by following along spiraling field lines, but within this X-region move poloidally only by the slower poloidal $E_r \times B_\phi$ drift due to the radial electric field. While the ions are slowly drifting poloidally across the almost-null B_θ X-region near the X-point, they are also drifting vertically due to curvature and grad-B drifts. For the configuration of Fig. 6 and Fig. 7, this vertical drift is downward towards the divertor. The time required to drift a radial distance Δr is

$$\tau_{\nabla B} = \frac{\Delta r}{V_{\nabla B,c}} = \frac{\Delta r}{(W_\perp + 2W_\parallel)/eRB} = \frac{eRB}{W(1+\zeta^2)}\Delta r \tag{30}$$

where ζ is the cosine of ion direction with respect to the magnetic field and W denotes the ion energy, and the poloidal $E_r \times B_\phi$ drift in this time is.

$$r(\theta_x)\Delta\theta = V_{E\times B}\tau_{\nabla B} = \frac{E_r(r)}{B_\phi}\frac{eRB}{W(1+\zeta^2)}\Delta r \tag{31}$$

Note that when the radial electric field changes sign (see Fig. 7), the directions of the poloidal drift and of the angular displacement both reverse.

The determination of the radial loss or transport of an ion that enters the X-region is a matter of calculating $\Delta\theta_n$ successively for all regions Δr_n between the radius of entry and the separatrix and summing. If the calculated sum becomes greater than $\Delta\theta_x$, or reverses sign, the ion has drifted out of the X-region back into the plasma at that radius—resulting in radial X-transport. These higher energy ions X-transported radially outward may then be ion-orbit lost [8].

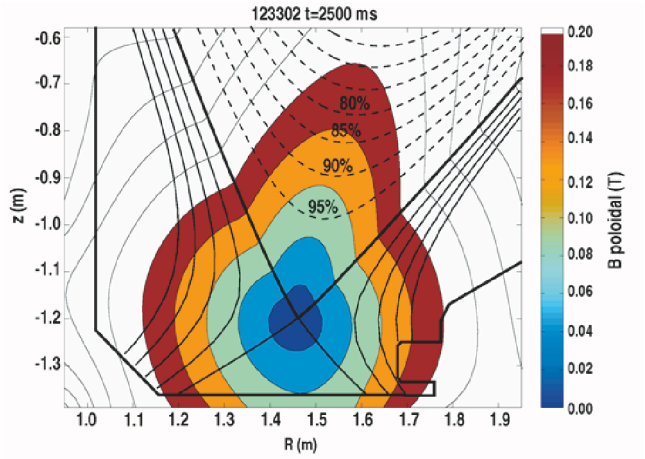

Fig. 6 Poloidal field in X-region for DIII-D shot [22].

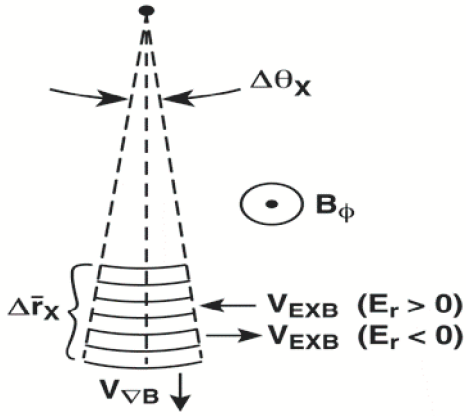

Fig. 7 Discretized X-region idealization [22].

Related work The models for outward convective flow in the presence of RMPs reviewed in [23] might be related to the reduction in inward pinch seen with RMP in this paper, and a mechanism similar to ion orbit loss was proposed for driving toroidal flow in [24].

Acknowledgements The contributions of C. Bae, T.G. Collart, T.E. Evans, J.-P. Floyd, B.A. Greirson, R.J. Groebner, M.-H. Sayer, M.T. Schumann, and T.M. Wilks are gratefully acknowledged. This work was supported in part by DoE Grant DE-FG02-ER54538.

References

[1] W.M. Stacey, Contrib. Plasma Phys. **48**, 94 (2008).
[2] W.M. Stacey, M.H. Sayer, J.P. Floyd, and R.J. Groebner, Phys. Plasmas **20**, 012509 (2013).
[3] W.M. Stacey and T.E. Evans, Nucl. Fusion **51**, 013007 (2011).
[4] T.M. Wilks, W.M. Stacey, and T.E. Evans, Phys. Plasmas **20**, 052505 (2013).
[5] J.P. Floyd, W.M. Stacey, R.J. Groebner, and S.Mellard, Phys. Plasmas **22**, 022508 (2015).
[6] J.P. Floyd and W.M. Stacey, Fusion Sci. & Techn. **61**, 227 (2012).
[7] W.M. Stacey, Contrib. Plasma Phys. **54**, 524 (2014).
[8] T.M. Wilks, W.M. Stacey, and T.E. Evans, presentation on Transport Task Force website (2015).
[9] W.M. Stacey, Phys. Plasmas **21**, 092517 (2014).
[10] W.M. Stacey and C. Bae, Phys. Plasmas **22**, 062503 (2015).
[11] S. Braginskii, Rev. Plasma Phys. (Consultants Bureau, New York, 1965), Vol 1, p. 205.
[12] W. M. Stacey, R. W Johnson, and J. Mandrekas, Phys. Plasmas **13**, 062508 (2006).
[13] C. Bae, W. M Stacey, and W. M Solomon, Nucl. Fusion **53**, 043011 (2013).
[14] T.G. Collart, MS Thesis, Ga. Inst. Techn. (2015); www.frc.gatech.edu.
[15] C. Bae, W.M. Stacey, S.G. Lee and L. Terzolo, Phys. Plasmas **21**, 022504 (2014).
[16] J.D. Callen, C.C. Hegna and A.J. Cole, Nucl. Fusion **53**, 113015 (2013).
[17] W.M. Stacey and B.A. Grierson, Nucl. Fusion **54**, 073021 (2014).
[18] W.M. Stacey and R.J. Groebner, Phys. Plasmas **15**, 012503 (2008).
[19] W.M. Stacey, Phys. Plasmas **18**, 102504 (2011).
[20] W.M. Stacey and M. T. Schumann, Phys. Plasmas **22**, 042504 (2015).
[21] W.M. Stacey, J.A. Boedo, T.E. Evans, B. A Grierson, and R. J. Groebner, Phys. Plasmas **19**, 112503 (2012).
[22] W.M. Stacey, Phys. Plasmas **18**, 122504 (2011).
[23] V. Rozhansky, Contrib. Plasma Phys. **6**, 508 (2014).
[24] V. Rozhansky, Plasma Phys. Control. Fusion. **54**, 102001 (2012).